Surfaces and Interfaces 26 (2021) 101386

Contents lists available at ScienceDirect

Surfaces and Interfaces

journal homepage: www.sciencedirect.com/journal/surfaces-and-interfaces

A comparative study of porous and hollow carbon nanofibrous structures from electrospinning for supercapacitor electrode material development

Kingsford Asare [a], Md Faruque Hasan [a], Abolghasem Shahbazi [b,*], Lifeng Zhang [a,*]

[a] Department of Nanoengineering, Joint School of Nanoscience and Nanoengineering, North Carolina A&T State University, 2907 E Gate City Blvd, Greensboro, NC 27401, USA

[b] Department of Natural Resources and Environmental Design, College of Agriculture and Environmental Sciences, North Carolina A&T State University, 1601 E Market St, Greensboro, NC 27411, USA

ARTICLE INFO

Keywords:
Carbon nanofiber
Nanostructure
Poly(methyl methacrylate)
Polyacrylonitrile
Supercapacitor
Electrospinning

ABSTRACT

Co-axial electrospinning is an efficient technique to develop core-shell or hollow nanofibrous structures. In this study electrospun carbon nanofibers with three different morphologies, i.e. solid nanofibers with porous structure (P-ECNF), hollow nanofibers with solid wall (H-ECNF), and hollow nanofibers with porous wall (HP-ECNF) were developed through bicomponent electrospinning and co-axial electrospinning of polyacrylonitrile (PAN) and poly (methyl methacrylate) (PMMA) by varying proportion of the sacrificial PMMA. Through comparative electrochemical analyses, it is revealed that the primary factors for electrochemical performance, i.e. specific capacitance, of the electrospun carbon nanofibrous materials are mesopore volume and total pore volume. The hollow structure as well as ordered carbon structure and intact fiber structure also benefits electrolyte transfer and subsequent electrochemical performance but is secondary. Overall the porous carbon nanofibrous electrode material from electrospinning PAN/PMMA (50/50) solution (P-ECNF-50-50) outperformed those hollow and hollow-porous counterparts from co-axial electrospinning and demonstrated the largest specific capacitance due to the largest mesopore volume as well as the largest total pore volume. This electrode material also showed excellent cycling stability (without any loss of specific capacitance) after 3,000 cycles of charging and discharging. It even showed some increase of specific capacitance with cycling test due to its relatively large amount of micropores.

1. Introduction

As a means of fortifying electric energy storage and supply, supercapacitors have shown competitive advantages in energy storage market owing to their high power density, cyclic stability and faster charge and discharge rates [1]. Supercapacitors can be classified into three main types: electric double layer capacitor (EDLC), pseudocapacitor, and hybrid capacitor. EDLC is able to provide ultrahigh power and outstanding cycling stability due to fast and non-destructive process between electrode and electrolyte [2,3]. Performance of supercapacitor depends crucially on the characteristics of electrode material and carbon has been largely used as electrode material for supercapacitor because of its electrical conductivity, chemical stability and low cost [4].

Carbon nanofibrous mat from electrospinning has been reported as promising electrode material for supercapacitor [5] because of its conductive network structure that can facilitate charge transfer [6] and advantage as stand-alone and binder-free electrode material for better electrochemical performance [7]. In general, carbon nanofibers from electrospinning of single precursor (e.g. polyacrylonitrile (PAN)) has solid structure, relatively low specific surface area, and correspondingly low EDLC capacitance [6]. In order to improve EDLC capacitance of electrospun carbon nanofibers (ECNFs), a number of research has been done to improve the specific surface area of ECNFs by creating porous or hollow structures [8]. For example, porous carbon nanofibers were prepared from ECNFs by in-situ activation with chemical agents such as H_3PO_4 [9], integration of nanoscale template followed by selective removal such as nano-$CaCO_3$ template [10], inclusion of sacrificial component such as poly(methyl methacrylate) (PMMA) [11] or use of PAN-based block copolymers for electrospinning and subsequent carbonization such as poly(acrylonitrile-block-methyl methacrylate) (PAN-b-PMMA) block copolymer [12]. In the meantime, electrode materials with hollow nanostructure have demonstrated their advantages

* Corresponding authors.
E-mail addresses: ash@ncat.edu (A. Shahbazi), lzhang@ncat.edu (L. Zhang).

https://doi.org/10.1016/j.surfin.2021.101386
Received 21 June 2021; Received in revised form 22 July 2021; Accepted 2 August 2021
Available online 9 August 2021

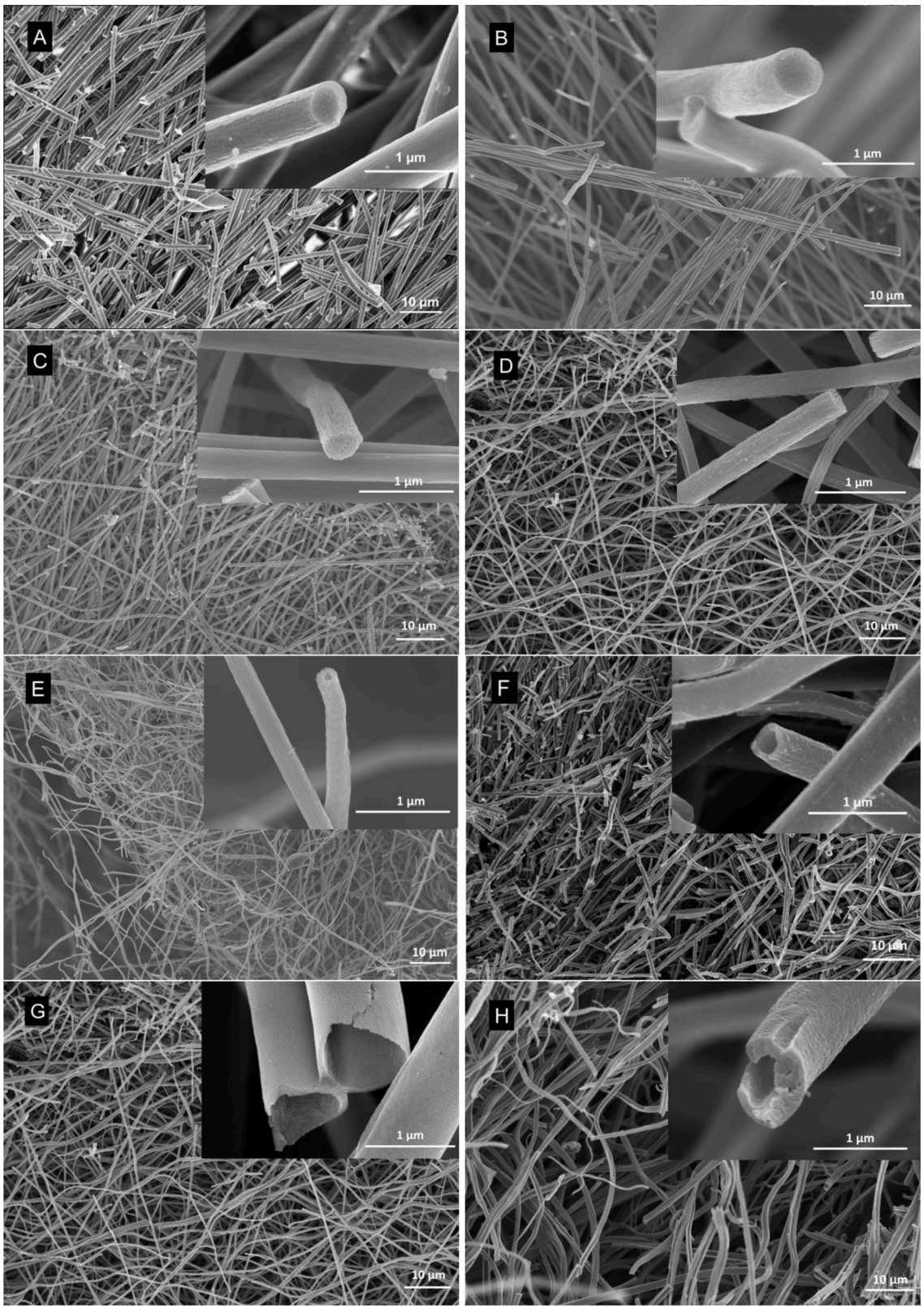

Fig. 1. Representative SEM images of electrospun carbon nanofibrous materials: (A) ECNF; (B) P-ECNF-90-10; (C) P-ECNF-70-30; (D) P-ECNF-50-50; (E) H-ECNF-10; (F) H-ECNF-20; (G) H-ECNF-30; (H) HP-ECNF-90-10; (I) HP-ECNF-70-30; (J) HP-ECNF-50-50.

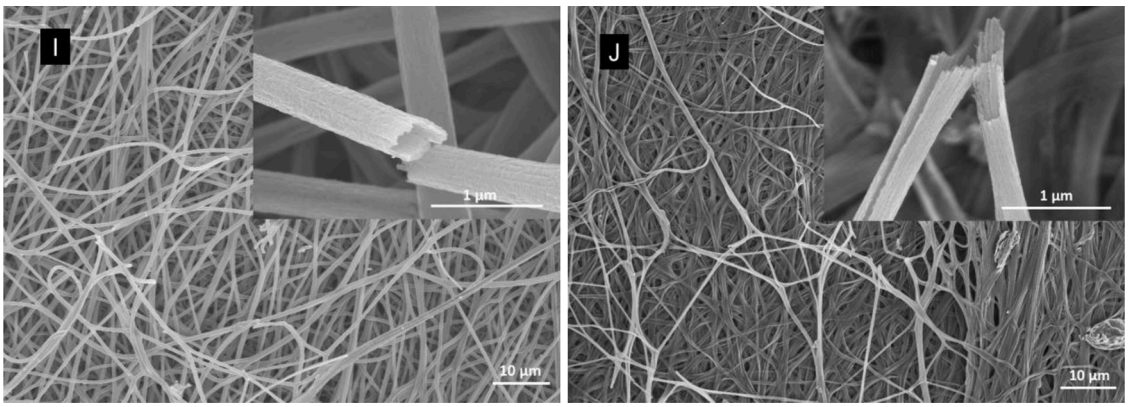

Fig. 1. (*continued*).

in supercapacitor applications by serving as "ion-buffering reservoirs" and reducing diffusion path of electrons and ions, which benefit corresponding electrochemical performance [13,14]. Co-axial electrospinning is a modified electrospinning process that involves simultaneous feeding two or more polymer solutions to mechanically aligned concentric nozzles for core-shell or hollow nanofibers [15]. In recent years, hollow ECNFs as well as porous hollow ECNFs have been developed through co-axial electrospinning and used as supercapacitor electrode materials [16–18]. Compared to that of solid ECNF, these porous and/or hollow ECNF electrode materials demonstrated improvement in electrochemical performance due to the formation of higher specific surface area for more charge storage sites.

It is noteworthy that all the above-mentioned research reported electrochemical performance of only one type of carbon nanostructure, i.e. porous, hollow, or porous hollow, and the electrochemical data are not comparable due to different electrospinning and electrochemical systems. It is still unknown if a certain 1D carbon nanostructure outperforms others to enhance electrochemical performance of supercapacitor under the same condition. For instance, hollow porous ECNF might outperform respective porous ECNF and hollow ECNF as electrode material for supercapacitor due to combined advantages of both porous and hollow nanostructures. However, there is no such conclusion or evidence yet. To verify this hypothesis, we prepared three types of carbon nanofibrous materials with respective porous, hollow, and hollow porous individual carbon nanofibers from electrospinning bicomponent PAN/PMMA solution and co-axial electrospinning PAN and PMMA as shell component and core component, respectively, based on the fact that PAN and PMMA have phase separation in PAN/PMMA bicomponent nanofibers and PMMA can decompose completely under heat and generate only volatile products as a sacrificial component [19] and conducted a side-by-side comparison for their electrochemical performance as electrode materials for EDLC supercapacitor. Solid carbon nanofibers from electrospinning of PAN were also prepared as a control sample. Our intention is to reveal the relationship between the structures of 1D carbon nanofibrous material from electrospinning including porous, hollow, and hollow porous structures and electrochemical performance of these carbon nanofibrous materials for supercapacitor electrode uses. The findings herein are expected to benefit the development of carbon electrode material from electrospinning for high-performance supercapacitors from the point view of 1D nanostructures.

2. Materials and methods

2.1. Materials

Polyacrylonitrile (PAN, $Mw = 1{,}50{,}000$), poly (methyl methacrylate) (PMMA, $Mw = 1{,}20{,}000$), potassium hydroxide (KOH) and N,N-dimethyl formamide (DMF) were purchased from Sigma Aldrich and used as received.

2.2. Carbon nanofiber preparation

Four types of carbon materials in the form of nanofibrous mat were prepared through electrospinning and co-axial electrospinning followed by stabilization and carbonization, i.e. solid carbon nanofibers (ECNF), porous carbon nanofibers (P-ECNF), hollow carbon nanofibers (H-ECNF), and hollow porous carbon nanofibers (HP-ECNF). ECNFs were electrospun from 12 wt.% PAN DMF solution. P-ECNFs were electrospun from 12 wt.% PAN/PMMA DMF solution with PAN/PMMA compositions at 90/10, 70/30 and 50/50 and denoted as P-ECNF-90-10, P-ECNF-70-30 and P-ECNF-50-50, respectively. All the electrospinning was conducted at 15 kV with a solution feed rate of 1 mL/h. To make H-ECNF and HP-ECNF, a co-axial electrospinning setup was used with certain polymer solutions for shell and core components, respectively. For H-ECNF, a fixed shell solution was maintained with 12 wt.% PAN in DMF and core solutions were PMMA solutions in DMF with varied concentrations at 10 wt.%, 20 wt.% and 30 wt. % and denoted as H-ECNF-10, H-ECNF-20, and H-ECNF-30, respectively. For HP-ECNF, a fixed core solution was maintained with 20 wt.% PMMA in DMF and shell solutions were 12 wt.% PAN/PMMA in DMF with varied PAN/PMMA compositions at 90/10, 70/30, and 50/50 and denoted as HP-ECNF-90-10, HP-ECNF-70-30 and HP-ECNF-50-50, respectively. All the co-axial electrospinning was conducted at 15 kV with feed rate of 1.5 mL/h for shell solution and 1 mL/h for core solution. Stabilization of as-spun nanofibrous mats was carried out in air at 280 °C for 6 h with a heating rate of 1 °C/min from room temperature. The stabilized nanofibrous mats were cooled down to room temperature and then heated in a nitrogen atmosphere to 900 °C with a heating rate of 5 °C/min. The nanofibrous mats were next maintained at 900 °C for 1 h before cooling down to room temperature. PMMA used herein is a sacrificial component, which completely decomposes during carbonization [19], and thus resulted in hollow and porous structures as described.

2.3. Characterizations

Morphology of the nanofibrous samples was examined using a Zeiss Auriga field emission scanning electron microscope (FESEM). BET specific surface area and BJH adsorption porosity of the nanofibrous samples were analyzed using a Micromeritics ASAP 2020 Surface Area and Porosity Analyzer. Raman spectroscopy was done at room temperature using a Horiba Raman Confocal Microscope at an excitation wavelength of 532 nm.

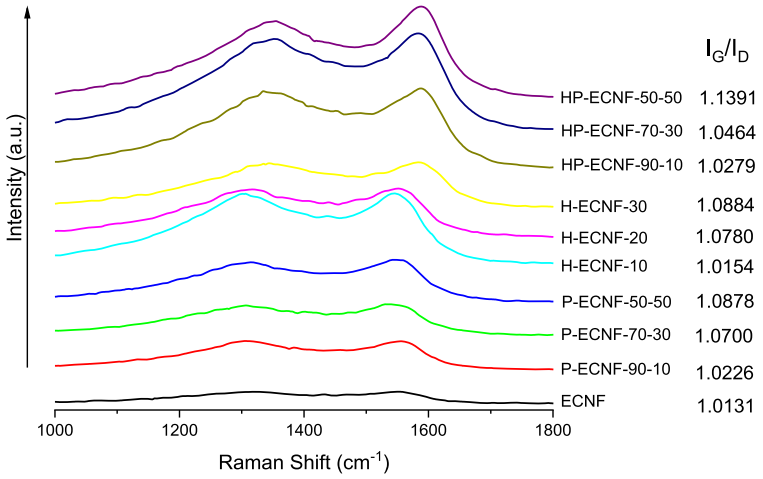

Fig. 2. Raman spectroscopy of the electrospun nanofibrous materials.

2.4. Electrochemical characterization

A square piece (1 cm × 1 cm) of each prepared carbon nanofibrous mat was cut and weighed. The square piece was then firmly attached to an Au working electrode using conductive carbon glue and placed in 6M KOH aqueous solution in combination with a reference electrode of Ag/AgCl and a counter electrode of platinum rod to construct a three-electrode electrochemical system, which was connected to a CH1660E electrochemical workstation for electrochemical measurement. Cyclic voltammetry (CV) test was conducted using a potential range of 0.0 to -0.8 V and a scan rate of 5, 10, 20, 50, 100 mV/s, respectively. The galvanostatic charge-discharge (CD) test was performed at a current density of 0.5, 1 and 2 A/g, respectively, in the potential range of 0.0 to -0.8 V. The specific capacitance was calculated based on both CV analysis from the following formula

$$C_{sp} = \frac{\int_{V_1}^{V_2} I(V)dV}{2 \times m \times \nu \times \Delta V}$$

where I is current, m is the mass of electrode material, ν is scan rate, and $\Delta V = V2 - V1$, which is the sweeping potential window (0.8 V) and CD analysis from the following formula

$$C_{sp} = \frac{I \times \Delta t}{m \times \Delta V}$$

where I is discharge current, m is mass of electrode material, Δt is discharge time, and ΔV is potential window (0.8 V).

Electrochemical impedance spectroscopy (EIS) test was performed within the frequency range of 100 kHz to 0.1 Hz. Cycling stability of the electrode materials was evaluated by 3000 cycles of CD test at 5 A/g within the potential window of 0.0 to -0.8 V.

3. Results and discussion

3.1. Morphology

ECNFs were solid fibers with an average diameter of 1034 ± 95 nm (Fig. 1A). P-ECNF showed porous structure both on surface and inside (Fig. 1B–D). At PAN/PMMA = 50/50, elongated pores and/or short channels were observed. With increase of PMMA content from PAN/PMMA = 90/10 to PAN/PMMA = 50/50, average fiber diameter reduced from 998 ± 91 nm for P-ECNF-90-10 to 679 ± 72 nm for P-ECNF-70-30 and to 565 ± 46 nm for P-ECNF-50-50. H-ECNF presented hollow structure as expected. H-ECNF-10, H-ECNF-20, and H-ECNF-30 exhibited increasing average fiber diameter from 513 ± 48 nm to 921 ± 89 nm and to 1679 ± 94 nm, respectively, with increase of PMMA concentration in core solution of co-axial electrospinning (Fig. 1E–G). The wall thickness of these hollow fibers is similar, i.e. 150–180 nm. HP-ECNF possessed a combined hollow and porous morphology (Fig. 1H–J), i.e. a hollow structure with porous wall. With increase of PMMA content in shell solution of co-axial electrospinning, average diameter of fiber reduced from 1588 ± 85 nm for HP-ECNF-90-10 to 782 ± 52 nm for HP-ECNF-70-30 and to 503 ± 59 nm for HP-ECNF-50-50. The wall thickness also reduced from ~200 nm to ~100 nm.

PMMA degrades and gasifies completely in temperature range of 300–400 °C [19]. Fiber size, porous structure, hollow channel size, and wall thickness in hollow nanofibers are dependent on balance of inflation effect due to discharge of relatively large volume of volatile PMMA degradation/gasification product in process of carbonization as well as volume shrinking effect due to PMMA removal and PAN carbonization. PAN and PMMA have polymer-polymer phase separation in the bicomponent nanofibers and domains of PMMA in PAN/PMMA bicomponent nanofibers can be completely removed in the process of carbonization. Larger proportion of PMMA would lead to larger volume shrinking during the carbonization process and reduce average fiber size in the case of P-ECNF. In the meantime, the larger proportion of PMMA could form elongated domain in the electrospinning process and result in "short channel" structure in carbonized fibers. As for H-ECNF, the larger size of hollow channel from higher PMMA concentration in core solution of co-axial electrospinning could be attributed to the larger amount of PMMA in core of the core-shell PAN/PMMA carbon precursor fibers, which generated larger volume of volatile products from PMMA degradation/gasification in the process of carbonization and counteracted the fiber contraction in that process and resulted in larger hollow channels. Porous wall structure of hollow nanofibers in the case of HP-ECNF could reduce thickness as well as mechanical strength of the wall and lead to huge size shrinkage/collapse in the process of carbonization. HP-ECNF-50-50 even showed some long and open slits on fiber surface.

3.2. Structure

Raman spectroscopy was used to characterize carbon structure of the electrospun carbon nanofibrous materials. The "D-band" between 1297 and 1355 cm^{-1} corresponds to the sp^3 hybridized disordered carbonaceous structures while the "G-band" between 1548 and 1591 cm^{-1} indicates the sp^2 hybridized graphitic phase of carbon [20]. The intensity ratio of I_G/I_D is used to characterize internal structure of these carbon nanofibrous materials. Among all the electrospun carbon nanofibrous materials, ECNF showed the least I_G/I_D value (Fig. 2). Compared to

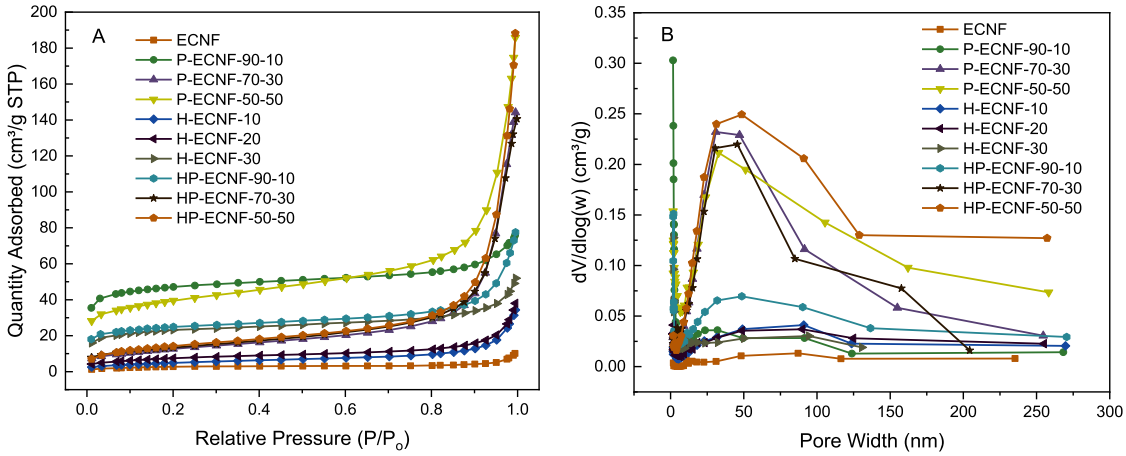

Fig. 3. N_2 adsorption isotherms (A) and pore size distributions (B) of electrospun carbon nanofibrous materials. The pore size distribution was obtained via the BJH adsorption.

Table 1
BET specific surface area and porosity of carbon nanofibrous materials.

Carbon nanofibrous materials	S_{BET} (m^2/g)	V_{micro} (cm^3/g)	V_{meso} (cm^3/g)	V_{macro} (cm^3/g)	V_{total} (cm^3/g)	BJH average pore size (nm)
ECNF	9.4	0.0006	0.0065	0.0053	0.0124	16.877
Pore proportion		4.8%	52.4%	42.7%		
P-ECNF-90-10	146	0.026	0.0637	0.0094	0.0991	3.582
Pore proportion		26.2%	64.3%	9.5%		
P-ECNF-70-30	45.9	0.0021	0.1706	0.0476	0.2204	19.173
Pore proportion		1.0%	77.4%	21.6%		
P-ECNF-50-50	130	0.01	0.2031	0.0633	0.2763	11.069
Pore proportion		3.6%	73.5%	22.9%		
H-ECNF-10	18.1	0.0014	0.0324	0.0164	0.0503	13.756
Pore proportion		2.8%	64.4%	32.6%		
H-ECNF-20	26.3	0.0023	0.0333	0.0188	0.0544	11.572
Pore proportion		4.2%	61.2%	34.6%		
H-ECNF-30	73.3	0.0068	0.0422	0.0103	0.0592	5.738
Pore proportion		11.5%	71.3%	17.4%		
HP-ECNF-90-10	78.8	0.0062	0.0722	0.0282	0.1066	8.604
Pore proportion		5.8%	67.7%	26.5%		
HP-ECNF-70-30	47.7	0.0015	0.1580	0.0545	0.2141	18.132
Pore proportion		0.7%	73.8%	25.5%		
HP-ECNF-50-50	51.5	0.0017	0.1877	0.0933	0.2827	24.790
Pore proportion		0.7%	66.4%	33%		

S_{BET} – BET specific surface area; V_{micro} – micropore volume; V_{meso} – mesopore volume; V_{macro} – macropore volume; V_{total} - total pore volume

ECNF, P-ECNF, H-ECNF and HP-ECNF all exhibited improved ordered carbon structure and larger amount of PMMA resulted in more ordered carbon structure. The addition of PMMA apparently facilitated PAN carbonization. This facilitation might be caused by PMMA's hydroxyl end groups, which could assist cyclization reaction of PAN molecules via an ionic mechanism [21] and consequently lower activation energy of the PAN cyclization reaction, reduce cyclization temperature, and increase enthalpy of the PAN cyclization process, allowing for the formation of more ordered carbon structures.

BET surface area and porosity analyses of the electrospun carbon nanofibrous materials were performed. N_2 adsorption isotherm as well as pore size distribution based on BJH adsorption of the electrospun carbon nanofibrous materials are shown in Fig. 3. The N_2 adsorption curves of these electrospun carbon nanofibrous materials can be classified as IUPAC Type II. The N_2 adsorption increase in low pressure region ($P/P_0 < 0.1$) indicated N_2 adsorption in micropores while the large N_2 adsorption increase in high pressure region ($P/P_0 > 0.9$) indicated N_2 adsorption in mesopores [22]. The N_2 adsorption curves as well as pore size distributions of the electrospun carbon nanofibrous materials suggested that P-ECNF-90-10, P-ECNF-50-50, H-ECNF-30, and HP-ENCF-90-10 possessed relatively large amount of micropores while all porous, hollow, and hollow porous samples showed significant amount of mesopores.

According to BET specific surface area and porosity results (Table 1), ECNF showed the lowest specific surface area and the smallest pore volume, indicating a solid fiber structure. P-ECNF demonstrated the largest specific surface area of 146 m^2/g with PAN/PMMA = 90/10 in the spinning solution. However, the corresponding pore volume is the smallest among the three P-ECNF samples. This is probably due to the micropore formation in the case of P-ECNF-90-10. In this case, PMMA formed much smaller domains in PAN/PMMA bicomponent nanofibers and resulted in the largest micropore volume among the three. With the increase of PMMA content in electrospinning solution, corresponding micropore volume reduced while mesopore and macropore volumes increased. Although P-ECNF-50-50 possessed the largest pore volume 0.2763 cm^3/g in this group, the largest proportion of pores is mesopores and the specific surface area is still less than that of P-ECNF-90-10. Compared to P-ECNF-90-10, P-ECNF-70-30 contains larger PMMA phase separation domains (less micropore volume) while compared to P-ECNF-50-50, P-ECNF-70-30 produces less amount of volatile product and creates less pores. The two factors together determined that P-ECNF-70-30 contains smaller pore volume (micropore, mesopore, macropore, and total pore volume) than that of P-ECNF-50-50 and thus smaller specific area than that of P-ECNF-50-50. H-ECNF possessed the least pore volume compared to P-ECNF and HP-ECNF, indicating a solid wall while their internal empty space does not contribute much to micro-, meso- or macro-porous structures. The pore volumes of all H-ECNF samples were close and there were some increases of total pore volume with the increase of PMMA concentration in core spinning solution. The total pore volumes of H-ECNF samples, however, were still more than 4 times of that of ECNF, indicating that the PAN/PMMA core-shell structure from co-axial electrospinning generated pores in the process of carbonization. This could be attributed to two reasons: (1) the partial mixing of PAN

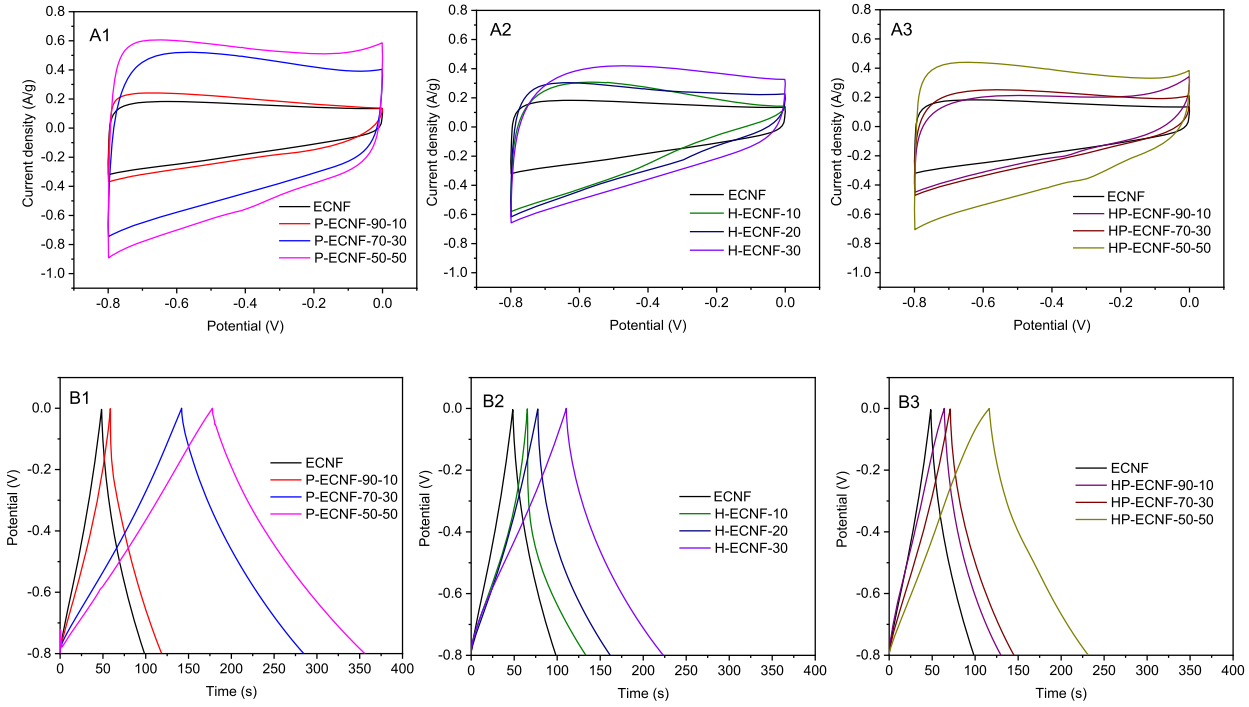

Fig. 4. Cyclic voltammetry (A) and galvanostatic charge-discharge (B) profiles of P-ECNF (labeled as 1), H-ECNF (labeled as 2), and HP-ECNF (labeled as 3). ECNF is used as reference in all plots.

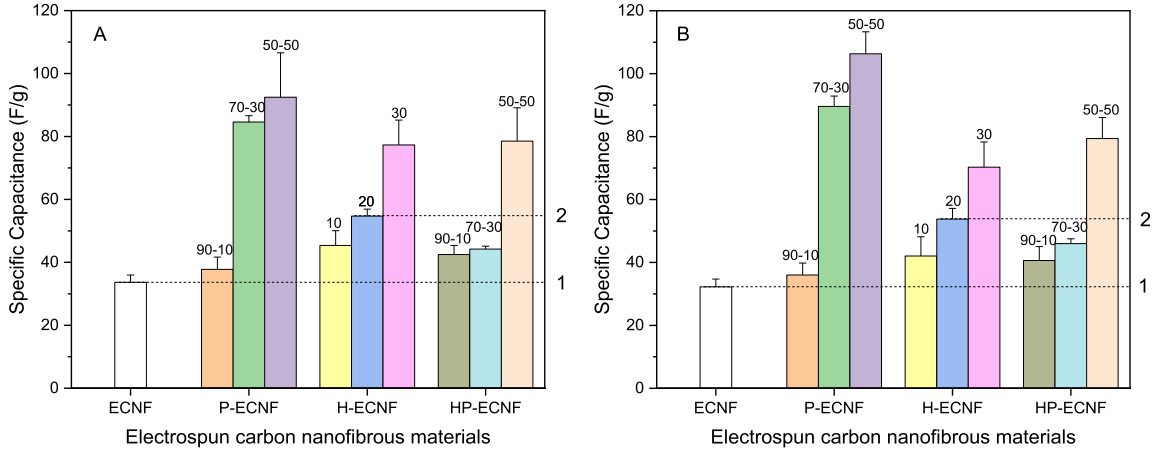

Fig. 5. Specific capacitances of electrospun carbon nanofibrous materials including ECNF, P-ECNF, H-ECNF, and HP-ECNF from cyclic voltammetry at 5 mV/s (A) and galvanostatic charge-discharge at 0.5 A/g (B). ECNF is used as a control of all the electrospun carbon nanofibrous materials and marked with line 1 while H-ECNF-20 is used as a control of all the HP-ECNF samples with fixed core solution of 20 wt.% PMMA in DMF and marked with line 2.

shell solution and PMMA core solution at interface of the Taylor cone in co-axial electrospinning due to common DMF solvent for both PAN and PMMA solutions. This kind of mixing could lead to very fine PAN-PMMA phase separation and resulted in different level of pores (micro-, meso-, and macro- pores) in final carbon nanofibers during carbonization; (2) the release of large volume of volatile products from PMMA degradation/gasification in the process of carbonization could also create pores. HP-ECNF combined the effects from P-ECNF and H-ECNF. Compared to H-ECNF-20, introduction of porous structure in wall increased specific surface area and pore volume. With increase of PMMA proportion in shell solution in co-axial electrospinning, micropore volume of HP-ECNF reduced with the increase of mesopore, macropore and total pore volumes. The specific surface area of HP-ECNF reduced with the increase of PMMA proportion in shell solution probably due to shrinkage and collapse of thin and porous wall in the process of carbonization.

3.3. *Electrochemical performance*

Electrochemical performance of all the electrospun carbon nanofibrous materials was evaluated by cyclic voltammetry (CV) and galvanostatic charge-discharge (CD) tests in 6M KOH electrolyte. CV profiles of these electrode materials at scan rate of 5 mV/s as well as their CD profiles at current density of 0.5 A/g are shown in Fig. 4. Their specific capacitances from both CV and CD were compared in Fig. 5 and generally match with each other. Compared to ECNF, all the porous and/or hollow nanostructures demonstrated better electrochemical performance. In each type of electrospun carbon nanofibrous material, i.e. P-ECNF, H-ECNF, and HP-ECNF, electrochemical performance increased with the content of PMMA in the spinning solution. With the largest PMMA content in spinning solution in each type of electrospun carbon nanofibrous material, sequence of electrical performance is P-

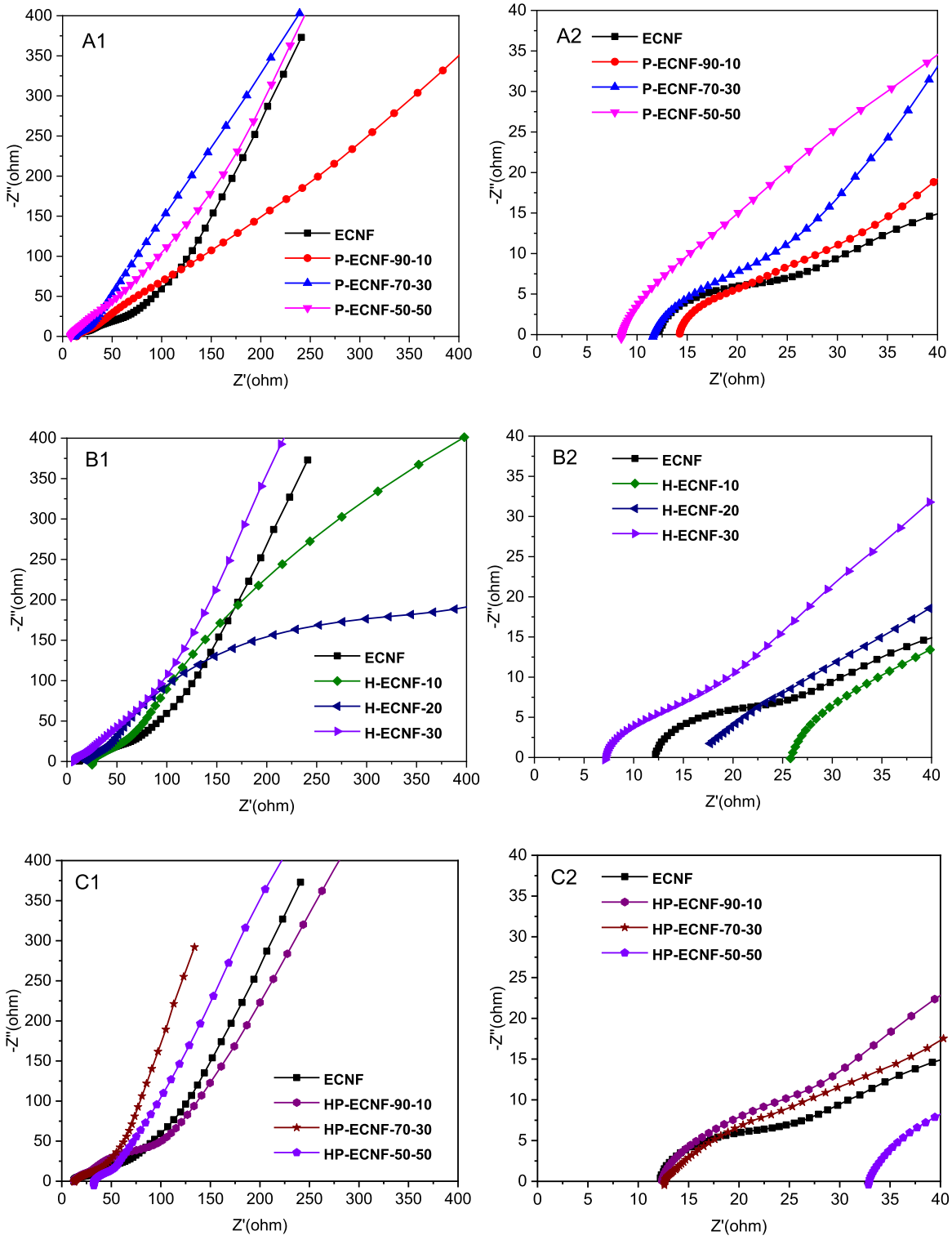

Fig. 6. Electrochemical impedance spectroscopy profiles of P-ECNF (A), H-ECNF (B), and HP-ECNF (C) in full frequency range (labeled as 1) and high frequency range (labeled as 2). ECNF is used as reference in all plots.

ECNF-50-50 > HP-ECNF-50-50 > H-ECNF-30.

Electrochemical impedance spectroscopy (EIS) has been extensively used to characterize electrode materials for supercapacitor [23]. Nyquist plots of all the electrospun carbon nanofibrous electrodes showed no or much depressed semi-circles at high frequency and nearly straight lines at low frequency (Fig. 6). For P-ECNF, the sample with the largest PMMA content in spinning solution (P-ECNF-50-50) exhibited the smallest electrode resistance (the intercept at the axis of real part of complex impedance) and the smallest electrolyte resistance (the size of semi-circle at high frequency) while the sample with the least PMMA content in spinning solution (P-ECNF-90-10) showed the largest electrode resistance, the largest electrolyte resistance and the least capacitive behavior (the angle between the straight line and the axis of real part of complex impedance). For H-ECNF, the sample with the largest

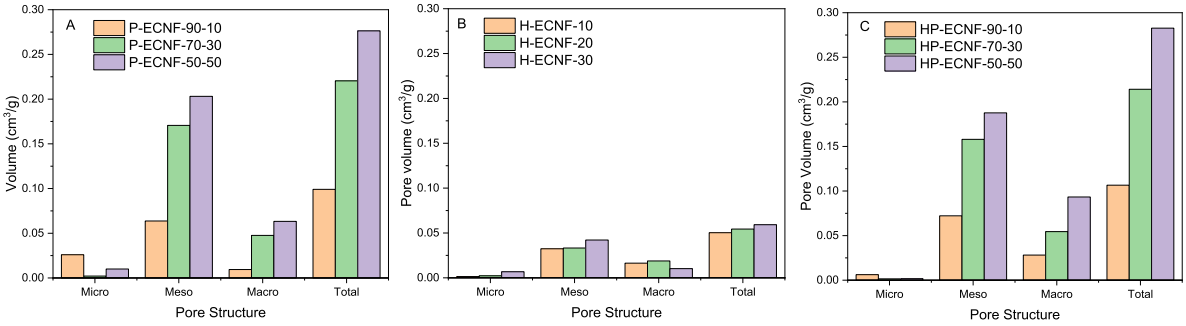

Fig. 7. Comparison of pore volumes of P-ECNF (A), H-ECNF (B), and HP-ECNF(C).

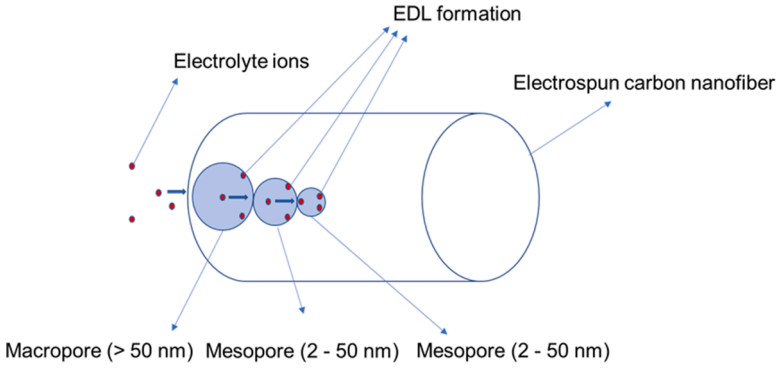

Fig. 8. Schematic diagram of electrolyte ion transfer in electrospun carbon nanofibers.

PMMA content in core spinning solution (H-ECNF-30) exhibited the lowest electrode resistance, the smallest electrolyte resistance and the best capacitive behavior. For HP-ECNF, the sample with the largest PMMA content in shell spinning solution (HP-ECNF-50-50) demonstrated the smallest electrolyte resistance but the largest electrode resistance.

The electrochemical performance of these electrospun carbon nanofibrous materials demonstrated a sequence: porous structure > hollow porous structure > hollow structure. Compared to the porous structure, the hollow structure did not demonstrate much advantage of the previously mentioned "ion-buffering reservoir" toward the specific capacitance. Electrochemical performance of these electrospun carbon nanofibrous materials did not correlate linearly with their specific surface area, indicating that multiple factors determine the electrochemical performance (specific capacitance) of these electrode materials instead of just specific surface area. These factors may include overall accessible surface area, electrolyte resistance, electrode resistance, and etc. It is observed that the samples with larger proportion of micropore volume such as P-ECNF-90-10 and HP-ECNF-90-10 possessed higher specific area but lower electrochemical performance in their respective groups. They also exhibited the largest electrolyte resistance. These indicated that electrolyte ions have more resistance to access micropores. In the meantime, the samples with the largest PMMA content in spinning solution in each group showed the largest pore volume particularly the largest mesopore volume and concurrently the best electrochemical performance. When specific capacitance of samples from each group are compared with corresponding sample's pore volume including micropore volume, mesopore volume, macropore volume and total pore

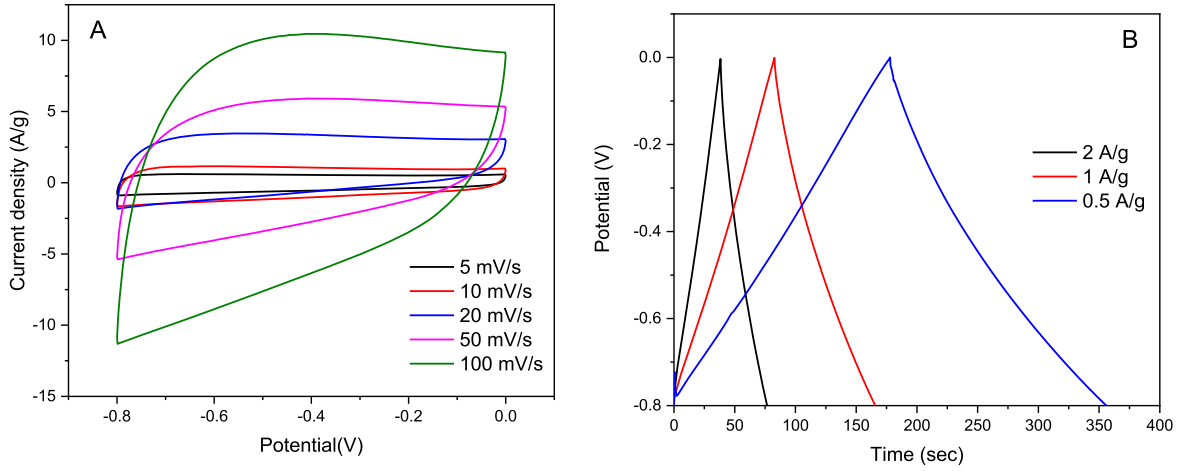

Fig. 9. Cyclic voltammetry (A) and galvanostatic charge-discharge (B) profiles of P-ECNF-50-50 at different scan rates (A) and current densities (B).

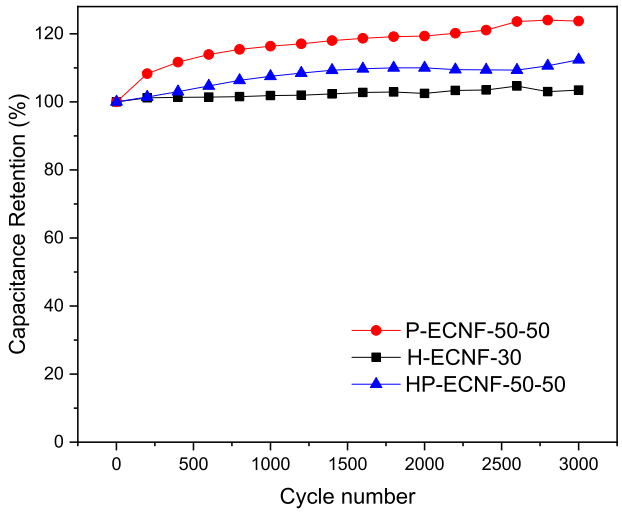

Fig. 10. Cycling stability of electrospun carbon nanofibrous electrode materials at current density of 5 A/g.

volume, it is observed that the mesopore volume and total pore volume follow the same sequence as that of specific capacitance for all the samples in each group (Fig. 7). Particularly in the case of P-ECNF, the specific capacitance is proportional to amount of mesopore volume (Coefficient of Determination, $R^2 = 0.99998$) and amount of total pore volume ($R^2 = 0.99293$) rather than the proportion of mesopore (%). These results indicated that mesopore volume and total pore volume are primary in determining electrochemical performance of these electrospun carbon nanofibrous electrode materials. Total pore volume determined the total number of available ion adsorption sites. Mesopore volume not only contributed to ion adsorption sites but also determined transportation difficulty of electrolyte ions to available adsorption sites. The mesopores could serve as connection paths and temporary reservoirs for electrolyte ions and assist electrolyte ions to access micropores for charge storage (Fig. 8). The mesopore volume sequence of our electrospun carbon nanofibrous electrode materials matched their electrolyte resistance sequence from EIS very well (Fig. 6). P-ECNF-50-50 possessed the highest mesopore volume and exhibited the highest electrochemical performance. When combine pore volume information with EIS results, it is also observed that micropore hindered electrolyte ion transport and increased electrolyte resistance while hollow structures facilitated electrolyte transport and reduced electrolyte resistance. The electrode resistance also played a role. Larger amount of PMMA in spinning solution led to more ordered carbon structure and could result in lower electrode resistance. However, electrode resistance of HP-ECNF-50-50 increased significantly. This might be due to the open long slits on HP-ECNF-50-50 nanofibers as observed from SEM (Fig. 1J) as well as the largest average pore size (Table 1), which reduced short moving paths of electron.

Furthermore the sample of P-ECNF-50-50 was further scanned at varied scan rates of 5–100 mV/s for CV test and performed CD test at varied current density of 0.5, 1 and 2 A/g, respectively (Fig. 9). With the increase of voltage sweep rate, the CV curves retained their quasi-rectangular shape. All the CD curves were almost linear and exhibited isosceles triangles. All these results indicated excellent supercapacitor behavior.

3.4. Cycling stability

Cycling stability of P-ECNF-50-50, H-ECNF-30, and HP-ECNF-50-50 was studied by monitoring the variation of specific capacitance with 3,000 cycles of CD test (Fig. 10). It is observed that there was almost no loss in specific capacitance for these nanofibrous electrode materials after 3000 cycles, indicating their long-term durability for supercapacitor use. Particularly P-ECNF-50-50 and HP-ECNF-50-50 even demonstrated some increases of specific capacitance during the cycling test. This could be attributed to improved wettability and electrode activation caused by continuous diffusion of electrolyte ions into previously inaccessible pores and graphitic layers, which led to an increase in active charge storage sites of the electrode. P-ECNF-50-50 possessed relatively large amount of micropores and these micropores may gradually become accessible for electrolyte ions with cycles. Therefore P-ECNF-50-50 exhibited the most increase of specific capacitance during the cycling test.

4. Conclusion

In this work, electrospun carbon nanofibrous materials with porous, hollow and hollow porous nanostructures were prepared through bicomponent electrospinning and co-axial electrospinning and comprehensively compared for their electrochemical performance as electrode materials for supercapacitor application. Co-axial electrospinning is efficient to generate hollow nanofibers as well as some intrinsic pore structures due to solution mixing at the interface of Taylor cone. Despite of the variation of morphology, i.e. porous nanostructure, hollow nanostructure, hollow porous nanostructure, mesopore volume and total pore volume are primary in determining electrochemical performance (specific capacitance) of these 1D carbon nanofibrous materials. Total pore volume determined the total number of available charge storage sites while mesopore volume controlled electrolyte resistance. Mesopores could serve as connection paths and temporary reservoirs for electrolyte ions and assist electrolyte ions to access micropores for charge storage. Hollow structure benefited electrolyte transport and reduced electrolyte resistance, but is not the decisive factor for electrochemical performance of the electrospun carbon nanofibrous electrode materials. Electrode resistance of these electrospun carbon nanofibrous materials also played a role in final electrochemical performance through their electrical resistance, which is dependent on carbon internal structure as well as overall fiber morphology.

CRediT authorship contribution statement

Kingsford Asare: Investigation, Methodology, Formal analysis, Writing – original draft. **Md Faruque Hasan:** Investigation, Methodology, Formal analysis, Writing – original draft. **Abolghasem Shahbazi:** Conceptualization, Resources, Funding acquisition. **Lifeng Zhang:** Conceptualization, Methodology, Resources, Writing – review & editing, Supervision, Project administration.

Declaration of Competing Interest

The authors declare that they have no known competing financial interests or personal relationships that could have appeared to influence the work reported in this paper.

Acknowledgments

This work was performed at the Joint School of Nanoscience and Nanoengineering of North Carolina A&T State University, a member of Southeastern Nanotechnology Infrastructure Corridor (SENIC) and National Nanotechnology Coordinated Infrastructure (NNCI), which is supported by the National Science Foundation (ECCS-1542174).

References

[1] B.K. Kim, S. Sy, A. Yu, J. Zhang, Electrochemical supercapacitors for energy storage and conversion. Handbook of Clean Energy Systems, John Wiley & Sons, 2015, pp. 1–25.

[2] P. Simon, Y. Gogotsi, Materials for electrochemical capacitors, Nat. Mater. 7 (2008) 845–854.
[3] S. Najib, E. Erdem, Current progress achieved in novel materials for supercapacitor electrodes: mini review, Nanoscale Adv. 1 (2019) 2817–2827.
[4] L.L. Zhang, X.S. Zhao, Carbon-based materials as supercapacitor electrodes, Chem. Soc. Rev. 38 (2009) 2520–2531.
[5] L. Zhang, A. Aboagye, A. Kelkar, C. Lai, H. Fong, A review: carbon nanofibers from electrospun polyacrylonitrile and their applications, J. Mater. Sci. 49 (2014) 463–480.
[6] A. Aboagye, Y. Liu, J.G. Ryan, J. Wei, L. Zhang, Hierarchical carbon composite nanofibrous electrode material for high-performance aqueous supercapacitors, Mater. Chem. Phys. 214 (2018) 557–563.
[7] C. Lai, Z. Zhou, L. Zhang, X. Wang, Q. Zhou, Y. Zhao, Y. Wang, X.F. Wu, Z. Zhu, H. Fong, Free-standing and mechanically flexible mats consisting of electrospun carbon nanofibers made from a natural product of alkali lignin as binder-free electrodes for high-performance supercapacitors, J. Power Sources 247 (2014) 134–141.
[8] B. Zhang, F. Kang, J.M. Tarascon, J.K. Kim, Recent advances in electrospun carbon nanofibers and their application in electrochemical energy storage, Prog. Mater. Sci. 76 (2016) 319–380.
[9] M. Zhi, S. Liu, Z. Hong, N. Wu, Electrospun activated carbon nanofibers for supercapacitor electrodes, RSC Adv. 4 (2014) 43619–43623.
[10] L. Zhang, Y. Jiang, L. Wang, C. Zhang, S. Liu, Hierarchical porous carbon nanofibers as binder-free electrode for high-performance supercapacitor, Electrochim. Acta 196 (2016) 189–196.
[11] G. He, Y. Song, S. Chen, L. Wang, Porous carbon nanofiber mats from electrospun polyacrylonitrile/polymethylmethacrylate composite nanofibers for supercapacitor electrode materials, J. Mater. Sci. 53 (2018) 9721–9730.
[12] Z. Zhou, T. Liu, A.U. Khan, G. Liu, Block copolymer-based porous carbon fibers, Sci. Adv. 5 (2019) eaau6852.
[13] S. Peng, L. Li, Y. Hu, M. Srinivasan, F. Cheng, J. Chen, S. Ramakrishna, Fabrication of spinel one-dimensional architectures by single-spinneret electrospinning for energy storage applications, ACS Nano 9 (2015) 1945–1954.
[14] K. Xu, S. Li, J. Yang, J. Hu, Hierarchical hollow MnO_2 nanofibers with enhanced supercapacitor performance, J. Colloid Interface Sci. 513 (2018) 448–454.
[15] D. Han, A.J. Steckl, Coaxial electrospinning formation of complex polymer fibers and their applications, ChemPlusChem 84 (2019) 1453–1497.
[16] Shilpa, A. Sharma, Free standing hollow carbon nanofiber mats for supercapacitor electrodes, RSC Adv. 6 (2016) 78528–78537.
[17] J.G. Kim, H.C. Kim, N.D. Kim, M.S. Khil, N-doped hierarchical porous hollow carbon nanofibers based on PAN/PVP@SAN structure for high performance supercapacitor, Compos. Part B 186 (2020), 107825.
[18] T.H. Le, Y. Yang, L. Yu, T. Gao, Z. Huang, F. Kang, Polyimide-based porous hollow carbon nanofibers for supercapacitor electrode, J. Appl. Polym. Sci. 133 (2016) 43397.
[19] L. Zhang, Y.L. Hsieh, Carbon nanofibers with nanoporosity and hollow channels from binary polyacrylonitrile systems, Eur. Polym. J. 45 (2009) 47–56.
[20] Z. Zhou, C. Lai, L. Zhang, Y. Qian, H. Hou, D.H. Reneker, H. Fong, Development of carbon nanofibers from aligned electrospun polyacrylonitrile nanofiber bundles and characterization of their microstructural, electrical, and mechanical properties, Polymer 50 (2009) 2999–3006.
[21] L. Zhang, Y.L. Hsieh, Nanoporous ultrahigh specific surface polyacrylonitrile fibres, Nanotechnology 17 (2006) 4416–4423.
[22] H.M. Lee, H.R. Kang, K.H. An, H.G. Kim, B.J. Kim, Comparative studies of porous carbon nanofibers by various activation methods, Carbon Lett. 14 (2013) 180–185.
[23] B.A. Mei, O. Munteshari, J. Lau, B. Dunn, L. Pilon, Physical interpretations of Nyquist plots for EDLC electrodes and devices, J. Phys. Chem. C 122 (2018) 194–206.